Energy levels of strained $In_xGa_{1-x}As$-GaAs superlattices

B. Jogai
Universal Energy Systems, Inc., 4401 Dayton-Xenia Road, Dayton, Ohio 45432

P. W. Yu
University Research Center, Wright State University, Dayton, Ohio 45435
(Received 16 November 1989; revised manuscript received 26 February 1990)

The complete $\mathbf{k}\cdot\mathbf{p}$ Hamiltonian with strain is solved numerically to obtain the energies and wave functions of $In_xGa_{1-x}As$-GaAs superlattices. The electron, heavy-hole, light-hole, and split-off bands are treated in a unified description in which the only adjustable parameters are the respective zone-center effective masses in each material. It is shown that the theory accurately reproduces the spectra of a wide range of published samples for valence-band offsets ranging from 0.3 to 0.6. It is also found that the transition energies are relatively insensitive to the valence-band offset over a wide range of offsets. The electron–light-hole exciton energy is fitted more closely at the lower offset values, and suggests a valence-band offset close to 0.4. At this offset, the light holes exhibit borderline type-II behavior, and are only slightly localized in the GaAs layers.

I. INTRODUCTION

In recent years there has been considerable interest in strained-layer $In_xGa_{1-x}As$-GaAs heterostructures.[1–9] This is a potentially attractive material system from a device perspective since the narrow band gap of $In_xGa_{1-x}As$ makes it useful as an infrared detector fabricated as a superlattice or quantum well. In addition, the low effective electron mass in $In_xGa_{1-x}As$ can be exploited in high-frequency transistor applications. Accordingly this material system has justifiably received a great deal of attention both theoretically and experimentally.

Despite detailed investigations, however, one of the most fundamental questions, the relative alignment of the conduction and valence bands along the growth axis, still remains unanswered. A related issue is whether the system is fully type I or mixed. In the mixed case the light holes exhibit type-II behavior, the heavy holes remain type I. Knowledge of the band alignment is vital if the transport and optical properties are to be accurately calculated. Unfortunately the valence (or conduction) -band offset cannot be observed directly, but is usually inferred from optical measurements such as photoluminescence excitation (PLE), absorption, and photoreflectance. By applying a suitable band-structure theory to calculate the energies, the valence-band offset is obtained by fitting the energy differences to the observed spectrum, treating the offset as an adjustable parameter. Based on this approach, Marzin *et al.*[1] estimated the valence-band offset as 0.3 for $x=0.15$, where the offset is defined as the fraction of the electron-heavy-hole (e-hh) band-gap difference appearing across the hh band edge. Taking into account the effects of strain, this offset leads naturally to the conclusion that the e-hh exciton is direct and the electron–light-hole (e-lh) exciton indirect in real space. This result was confirmed by Ji *et al.*[6] using a similar model to fit their data for x varying from 0.13 to 0.193. Pan *et al.*[8] were also able to fit their data to a valence-band offset of 0.3 for $x=0.11$. Significantly different results were obtained by Menendez *et al.*,[7] who claim an offset of 0.6 for $x=0.05$. At this offset the light-hole exciton will also be direct in real space, a result that is in obvious disagreement with previous works. Recent measurements by Ksendzov *et al.*[10] for $x=0.11$ and 0.19 appear to agree with this conclusion. In order to accommodate such widely differing results, Joyce *et al.*[9] have proposed that the band offset is a function of x, varying from 0.6 for $x<0.05$ to 0.2 for $x>0.2$. This, however, does not explain the discrepancy between the results of Ksendzov *et al.*[10] on the one hand and Ji *et al.*[6] and Pan *et al.*[8] on the other, for $0.11<x<0.193$. The apparent discrepancy for samples of similar mole fractions would suggest a sample-dependent band offset, a deduction that may be probable in view of the proposal[10] that the offset is very sensitive to the position of the As atom near the interface.

But before concluding that the offset is nearly unpredictable due to random effects at the interface, it is worthwhile to examine other possibilities. One such possibility is the theory used to fit the data. The aim of the present work is to point out the shortcomings of the effective-mass model currently used to calculate the energies, and to present a more detailed model which can be used to fit the spectra of a wide range of samples. So far the accepted approach has been to use Marzin's[11] extension of Bastard's[12] envelope-function approximation (EFA) to include the effects of strain. This, however, is subject to all of the limitations inherent in the EFA which, as pointed out by Schuurmans and 't Hooft,[13] is an oversimplification of Kane's complete $\mathbf{k}\cdot\mathbf{p}$ model.[14] The important free electron terms on the diagonal of the $\mathbf{k}\cdot\mathbf{p}$ Hamiltonian are omitted. These, it turns out, are actually larger than the off-diagonal terms retained in the EFA. In addition, the coupling between the lh and split-off (SO) bands is disregarded. Marzin[11] includes only the

strain-induced lh-SO coupling. The only available adjustable parameters are the momentum matrix element between the host Bloch functions at the zone center and the valence-band offset. The matrix element is calculated from the effective mass and band gap,[14] and is derived by fitting the band structure determined from the unstrained EFA Hamiltonian to the known band structure of the host bulk materials. But because of the approximations made, the matrix element must be assigned different values corresponding to each band, as described in Ref. 13. Hence the e, lh, and SO states must be obtained individually, each time with a different matrix element. The hh states, dispersionless within the EFA, are found separately after reintroducing the free electron term.

Such a disjointed approach can lead to imprecise and inconsistent calculations. With only the matrix element to manipulate, it is not possible to fit the spectra of different samples for a fixed offset; it is also necessary to vary the offset. The final result depends strongly on the choice of effective masses as well as the offset. It is not surprising, therefore, that such widely varying offsets have been estimated for somewhat similar samples.

In this paper we present a unified method, adding the effects of strain to the more complete $\mathbf{k}\cdot\mathbf{p}$ Hamiltonian of Schuurmans and 't Hooft[13] and Eppenga *et al.*[15] A novel technique is used to solve the resulting Hamiltonian. With more parameters available for adjustments, we find that the outcome does not depend as strongly on the offset as in the modified EFA. In fact, for a given set of effective masses and an offset of 0.4, we have been able to fit the data of all the samples of Refs. 1 and 6–8 very accurately. In addition, we have varied the offset from 0.3 to 0.6 and found that the change of the calculated transition energies is negligible in many instances. We find that the energy differences are not as sensitive to the offset as previously supposed. We also show that for a 0.4 offset the lh ground state is extended over the entire superlattice period due to the small lh band-edge discontinuity, and is only slightly localized in the GaAs layer. Because the lh aspect of the superlattice is borderline type II if a 0.4 offset is presumed, it is relatively easy to form a e-lh exciton under this condition. This may explain the strong e-lh excitonic peak reported in Ref. 7.

In the following section we describe the $\mathbf{k}\cdot\mathbf{p}$ model modified to include the effects of strain, the interface boundary conditions, and the method of solution. Comparison of the calculated spectra with experimental data is presented in Sec. III. The results are summarized in Sec. IV.

II. THEORY

Consider a superlattice composed of layers l where $l=1$ denotes the GaAs layers and $l=2$ the $In_xGa_{1-x}As$ layers. We choose z as the quantization axis of angular momenta as well as the growth axis and let x and y denote two orthogonal axes in the $z=0$ plane. We deal only with the case in which the crystal momentum in the x-y plane is zero. Then in a Kane-type $\mathbf{k}\cdot\mathbf{p}$ analysis the 8×8 Hamiltonian in the Γ-point basis is reduced to two degenerate 4×4 blocks. For the "spin-up" block the basis set is $u_e=|s\uparrow\rangle$, $u_{hh}=|\frac{3}{2},\frac{3}{2}\rangle$, $u_{lh}=|\frac{3}{2},\frac{1}{2}\rangle$, and $u_{SO}=|\frac{1}{2},\frac{1}{2}\rangle$. There is an analogous "spin-down" set. In material l the energies of the spin-up states for a given k_z are given by the eigenvalues of the matrix $\underline{H}^l$,[13,15]

$$\underline{H}^l=\begin{bmatrix} E_s^l+s^l\alpha k_z^2 & 0 & -\sqrt{\frac{2}{3}}iP^lk_z & \sqrt{\frac{1}{3}}iP^lk_z \\ 0 & E_p^l-(\gamma_1^l-2\gamma_2^l)\alpha k_z^2 & 0 & 0 \\ \sqrt{\frac{2}{3}}iP^lk_z & 0 & E_p^l-(\gamma_1^l+2\gamma_2^l)\alpha k_z^2 & 2\sqrt{2}\gamma_2^l\alpha k_z^2 \\ -\sqrt{\frac{1}{3}}iP^lk_z & 0 & 2\sqrt{2}\gamma_2^l\alpha k_z^2 & E_p^l-\Delta^l-\gamma_1^l\alpha k_z^2 \end{bmatrix}, \tag{1}$$

where E_s^l (E_p^l) is the unstrained conduction (valence) -band-edge energy, $\alpha=\hbar^2/2m$, P^l is Kane's momentum matrix element,[14] and Δ^l is the spin-orbit energy. The layer-dependent constants s^l, γ_1^l, and γ_2^l are Luttinger-type parameters.[16] These along with P^l are obtained for $l=1$ and 2 by diagonalizing H^l and fitting the resulting energy dispersion relations to those of the respective bulk materials, i.e., by equating the Γ-point effective masses derived from the dispersion relations to the experimentally determined effective masses of each material.

We consider the superlattice grown on a GaAs buffer layer in the [001] orientation. For growth on a thick GaAs buffer, the $In_xGa_{1-x}As$ layers are subject to an in-plane biaxial compression, a consequence of having to assume the GaAs lattice constant. This effect increases the overall band gap in the $In_xGa_{1-x}As$ layers. In addition, the uniaxial strain along the growth axis splits the degeneracy between the $|\frac{3}{2},\frac{3}{2}\rangle$ and $|\frac{3}{2},\frac{1}{2}\rangle$ states. The strain Hamiltonian in the $|J,m_J\rangle$ basis is given for each layer by[17,18]

$$\underline{H}_{st}^l=\begin{bmatrix} 0 & 0 & 0 & 0 \\ 0 & -\delta E_H^l-\frac{1}{2}\delta E_s^l & 0 & 0 \\ 0 & 0 & -\delta E_H^l+\frac{1}{2}\delta E_s^l & \frac{1}{\sqrt{2}}\delta E_s^l \\ 0 & 0 & \frac{1}{\sqrt{2}}\delta E_s^l & -\delta E_H^l \end{bmatrix}, \tag{2}$$

where δE_H^l is the shift of the "center of gravity" of the $|J,m_J\rangle$ states relative to the $|s\uparrow\rangle$ states due to the hydrostatic component of the strain and δE_s^l is the shear component. The elements of H_{st}^l are obtained from[18]

$$\delta E_H^l=a^l(e_{xx}^l+e_{yy}^l+e_{zz}^l) \tag{3}$$

and

$$\delta E_s^l = 2b^l(e_{zz}^l - e_{xx}^l) , \tag{4}$$

in which a^l is the hydrostatic deformation potential, b^l is the valence-band axial deformation potential, and e_{ij}^l are elements of the strain tensor. The nonzero elements of the strain tensor are

$$e_{xx}^l = e_{yy}^l = (d^{(1)} - d^l)/d^l , \tag{5}$$

$$e_{zz}^l = -(2C_{12}^l/C_{11}^l)e_{xx}^l , \tag{6}$$

where C_{11}^l and C_{12}^l are elements of the elastic stiffness tensor, and d^l is the lattice constant of material l. The hydrostatic deformation potential is found from

$$a^l = -\frac{(C_{11}^l + 2C_{12}^l)}{3}\frac{\partial E_g^l}{\partial P} , \tag{7}$$

where $\partial E_g^l/\partial P$ is the pressure dependence of the band gap. From Eq. (5) it is seen that the strain Hamiltonian for the GaAs layers is a null matrix.

We define the strained band gap as

$$E_{gs}^l = E_g^l + \delta E_H^l + \tfrac{1}{2}\delta E_s^l . \tag{8}$$

Taking the strain into account, the energy of the $|\frac{3}{2},\frac{3}{2}\rangle$ states is given by

$$E_{p'}^l = E_p^l - \delta E_H^l - \tfrac{1}{2}\delta E_s^l . \tag{9}$$

From the strained band gaps and assuming the valence-band offset to be Q_v we obtain

$$E_{p'}^l = Q_v(E_{gs}^{(2)} - E_{gs}^l) , \tag{10}$$

$$E_s^l = E_{p'}^l + E_{gs}^l . \tag{11}$$

The composition-dependent bulk band gaps in units of eV are estimated from[19–21]

$$E_g(300\text{ K}) = 1.43 - 1.53x + 0.45x^2 , \tag{12a}$$

$$E_g(77\text{ K}) = 1.508 - 1.47x + 0.375x^2 , \tag{12b}$$

$$E_g(2\text{ K}) = 1.5192 - 1.5837x + 0.475x^2 . \tag{12c}$$

It is clear from Eqs. (9)–(11) that the valence-band offset is defined with respect to the hh states in the two layers. In addition, the "zero" of energy is taken as the energy of the hh states is $In_xGa_{1-x}As$. Combining Eqs. (1) and (2) and substituting for E_s^l and E_p^l, the total Hamiltonian becomes

$$\underline{H}_{\text{tot}} = \begin{pmatrix} E_{p'}^l + E_{gs}^l + s^l\alpha k_z^2 & 0 & -\sqrt{\tfrac{2}{3}}iP^lk_z & \sqrt{\tfrac{1}{3}}iP^lk_z \\ 0 & E_{p'}^l - (\gamma_1^l - 2\gamma_2^l)\alpha k_z^2 & 0 & 0 \\ \sqrt{\tfrac{2}{3}}iP^lk_z & 0 & E_{p'}^l + \delta E_s^l - (\gamma_1^l + 2\gamma_2^l)\alpha k_z^2 & 2\sqrt{2}\gamma_2^l\alpha k_z^2 + \dfrac{1}{\sqrt{2}}\delta E_s^l \\ -\sqrt{\tfrac{1}{3}}iP^lk_z & 0 & 2\sqrt{2}\gamma_2^l\alpha k_z^2 + \dfrac{1}{\sqrt{2}}\delta E_s^l & E_{p'}^l - \Delta^l + \tfrac{1}{2}\delta E_s^l - \gamma_1^l\alpha k_z^2 \end{pmatrix} . \tag{13}$$

The Hamiltonian of Eq. (13) is Fourier transformed and solved in real space, in which k_z is transformed to $-i\partial/\partial z$ and k_z^2 to $-\partial^2/\partial z^2$. The resulting coupled differential equations satisfy

$$\underline{H}_{\text{tot}}\left[k_z \rightarrow -i\frac{\partial}{\partial z}\right]\mathbf{F} = E\mathbf{F} , \tag{14}$$

where E is the energy and $\mathbf{F}$ is the column vector $\{F_e, F_{\text{hh}}, F_{\text{lh}}, F_{\text{SO}}\}$. Each F is the slowly varying envelope portion of the wave function

$$\psi^l(\mathbf{r}) = \sum_j u_j^l(\mathbf{r})F_j(z)e^{i(k_x x + k_y y)} , \tag{15}$$

where $u_j^l(\mathbf{r})$ is the cell-periodic part of the host Bloch function at the zone center and the subscript j runs over the four bands.

Equation (14) is best solved as a coupled entity. Among the previous efforts in this area is that of Porod *et al.*,[22] who had solved a similar set for the GaAs-$Al_xGa_{1-x}As$ system. To make a numerical treatment feasible they found it necessary to decouple the system of equations, retaining terms only up to second order in $\partial/\partial z$. But this results in a peculiar eigenvalue problem in which each decoupled equation is nonlinear in energy. Hence the eigenvalues must be obtained self-consistently. A further disadvantage is that valuable terms necessary to match the interface boundary conditions are lost. A different scheme was used by Altarelli,[23] who retained all of the important terms, and expanded the components of ψ in a suitable basis set. The system was subsequently reduced to a generalized eigenvalue problem to be solved for the energies and the envelope expansion coefficients. This, however, requires some guesswork in selecting the basis set. Besides, errors are inevitably incurred by having to truncate the set. A more exact approach was employed by Schuurmans and 't Hooft[13] and is similar to that described in Ref. 24 in the treatment of piecewise-constant potentials. At each interface the boundary conditions are implemented by using transfer matrices. The composition of these matrices is dictated by the need to enforce the continuity of the envelope functions and particle current across each interface. A polynomial of degree 8 in the crystal momentum is obtained, and the energies are computed indirectly from its roots. One disadvantage of this scheme, apart from being a rather difficult problem, is that some of the solutions are physically unrealistic, as explained in Ref. 13.

We have opted for a more fundamental technique wherein the superlattice period is divided into N equispaced points separated by Δz. The differential operators in Eq. (14) are then represented by their finite difference equivalents, reducing the system to the eigenvalue problem

$$\begin{bmatrix} \underline{M}_{11} & \underline{0} & \underline{M}_{13} & \underline{M}_{14} \\ \underline{0} & M_{22} & \underline{0} & \underline{0} \\ \underline{M}_{31} & \underline{0} & \underline{M}_{33} & \underline{M}_{34} \\ \underline{M}_{41} & \underline{0} & \underline{M}_{43} & \underline{M}_{44} \end{bmatrix} \begin{bmatrix} \mathbf{F}_e \\ \mathbf{F}_{hh} \\ \mathbf{F}_{lh} \\ \mathbf{F}_{SO} \end{bmatrix} = E \begin{bmatrix} \mathbf{F}_e \\ \mathbf{F}_{hh} \\ \mathbf{F}_{lh} \\ \mathbf{F}_{SO} \end{bmatrix} , \tag{16}$$

where each $\underline{M}$ represents an $N\times N$ matrix, each $\mathbf{F}$ is a column vector of length N, and $\underline{0}$ is an $N\times N$ null matrix. Because we have not included the hh-lh mixing, the hh component of the matrix is in block diagonal form. The eigenvalues are readily obtained by diagonalizing the large matrix. On finding the eigenvectors of the large matrix, the rows will contain the envelope functions in the order indicated in Eq. (16). For example, the first N rows will consists of $\mathbf{F}_e$.

The interface boundary conditions to be applied, apart from the continuity of the envelope functions, are obtained by integrating Eq. (14) across the interface. Equation (14) can be written

$$\mathbf{A}\frac{\partial^2\mathbf{F}}{\partial z^2}+\mathbf{B}\frac{\partial\mathbf{F}}{\partial z}+\mathbf{C}\mathbf{F}=\underline{\mathbf{0}} , \tag{17}$$

where $\mathbf{A}$, $\mathbf{B}$, and $\mathbf{C}$ are 4×4 matrices and $\mathbf{F}$ is a column vector. Assuming that the interface is at $z=0$ and taking advantage of the piecewise-constant nature of the matrices, Eq. (17) may be expressed as

$$(A^{(2)}-A^{(1)})\theta(z)\frac{\partial^2\mathbf{F}}{\partial z^2}+\mathbf{A}^{(1)}\frac{\partial^2\mathbf{F}}{\partial z^2} +(\mathbf{B}^{(2)}-\mathbf{B}^{(1)})\theta(z)\frac{\partial\mathbf{F}}{\partial z}+\mathbf{B}^{(1)}\frac{\partial\mathbf{F}}{\partial z} +(\mathbf{C}^{(2)}-\mathbf{C}^{(1)})\theta(z)\mathbf{F}+\mathbf{C}^{(1)}\mathbf{F}=\underline{\mathbf{0}} , \tag{18}$$

where the unit step function $\theta(z)=1$ for $z>0$ and $\theta(z)=0$ for $z<0$. Integrating Eq. (18) across an infinitesimally small interval spanning the interface and using $\dot{\theta}(z)=\delta(z)$ we obtain

$$\mathbf{A}^{(2)}\frac{\partial\mathbf{F}}{\partial z}(0^+)-\mathbf{A}^{(1)}\frac{\partial\mathbf{F}}{\partial z}(0^-)-(\mathbf{A}^{(2)}-\mathbf{A}^{(1)})\frac{\partial\mathbf{F}}{\partial z}(0) +\mathbf{B}^{(2)}\mathbf{F}(0^+)-\mathbf{B}^{(1)}\mathbf{F}(0^-)-(\mathbf{B}^{(2)}-\mathbf{B}^{(1)})\mathbf{F}(0)=\underline{\mathbf{0}} . \tag{19}$$

The boundary conditions implied by Eq. (19) cannot be imposed in practice because we do not know the function and its derivative at $z=0$. As yet, there is no satisfactory way of implementing the boundary conditions at an abrupt interface as discussed in Refs. 13 and 23, and by Morrow and Brownstein.[25] Fortunately the interface is never completely abrupt in practice, so that within a small interval on either side, the parameters s^l, γ_1^l, γ_2^l, and P^l are expected to vary smoothly. This allows us to discard the terms to be evaluated at $z=0$ in Eq. (19), yielding

$$\mathbf{A}^{(2)}\frac{\partial\mathbf{F}}{\partial z}(0^+)-\mathbf{A}^{(1)}\frac{\partial\mathbf{F}}{\partial z}(0^-)+\mathbf{B}^{(2)}\mathbf{F}(0^+) -\mathbf{B}^{(1)}\mathbf{F}(0^-)=\underline{\mathbf{0}} . \tag{20}$$

In the finite difference scheme this is applied by the transformation

$$\mathbf{A}(z)\frac{\partial^2}{\partial z^2}\rightarrow\frac{\partial}{\partial z}\mathbf{A}(z)\frac{\partial}{\partial z} . \tag{21}$$

Equation (16) is then approximated by

$$(E_{p'}^i+E_{gs}^i)F_e^i-\alpha\left[\frac{s^{i+1}-s^{i-1}}{2\Delta z}\right]\left[\frac{F_e^{i+1}-F_e^{i-1}}{2\Delta z}\right]-\alpha s^i\frac{F_e^{i+1}-2F_e^i+F_e^{i-1}}{(\Delta z)^2} -\sqrt{\tfrac{2}{3}}P^i\frac{F_{lh}^{i+1}-F_{lh}^{i-1}}{2\Delta z}+\sqrt{\tfrac{1}{3}}P^i\frac{F_{SO}^{i+1}-F_{SO}^{i-1}}{2\Delta z}=EF_e^i , \tag{22a}$$

$$E_{p'}^iF_{hh}^i+\alpha\left[\frac{\gamma_1^{i+1}-2\gamma_2^{i+1}-\gamma_1^{i-1}+2\gamma_2^{i-1}}{2\Delta z}\right]\left[\frac{F_{hh}^{i+1}-F_{hh}^{i-1}}{2\Delta z}\right]+\alpha(\gamma_1^i-2\gamma_2^i)\frac{F_{hh}^{i+1}-2F_{hh}^i+F_{hh}^{i-1}}{(\Delta z)^2}=EF_{hh}^i , \tag{22b}$$

$$\sqrt{\tfrac{2}{3}}P^i\frac{F_e^{i+1}-F_e^{i-1}}{2\Delta z}+(E_{p'}^i+\delta E_s^i)F_{lh}^i+\alpha\left[\frac{\gamma_1^{i+1}+2\gamma_2^{i+1}-\gamma_1^{i-1}-2\gamma_2^{i-1}}{2\Delta z}\right]\left[\frac{F_{lh}^{i+1}-F_{lh}^{i-1}}{2\Delta z}\right] +\alpha(\gamma_1^i+2\gamma_2^i)\frac{F_{lh}^{i+1}-2F_{lh}^i+F_{lh}^{i-1}}{(\Delta z)^2}-2\sqrt{2}\alpha\left[\frac{\gamma_2^{i+1}-\gamma_2^{i-1}}{2\Delta z}\right]\left[\frac{F_{SO}^{i+1}-F_{SO}^{i-1}}{2\Delta z}\right] -2\sqrt{2}\gamma_2^i\frac{F_{SO}^{i+1}-2F_{SO}^i+F_{SO}^{i-1}}{(\Delta z)^2}+\frac{1}{\sqrt{2}}\delta E_s^iF_{SO}^i=EF_{lh}^i , \tag{22c}$$

$$-\sqrt{\tfrac{1}{3}}P^i\frac{F_e^{i+1}-F_e^{i-1}}{2\Delta z}-2\sqrt{2}\alpha\left[\frac{\gamma_2^{i+1}-\gamma_2^{i-1}}{2\Delta z}\right]\left[\frac{F_{\rm lh}^{i+1}-F_{\rm lh}^{i-1}}{2\Delta z}\right]+\frac{1}{\sqrt{2}}\delta E_s^i F_{\rm lh}^i+(E_{p'}^i-\Delta^i+\tfrac{1}{2}\delta E_s^i)F_{\rm SO}^i$$

$$+\alpha\left[\frac{\gamma_1^{i+1}-\gamma_1^{i-1}}{2\Delta z}\right]\left[\frac{F_{\rm SO}^{i+1}-F_{\rm SO}^{i-1}}{2\Delta z}\right]+\alpha\gamma_1^i\frac{F_{\rm SO}^{i+1}-2F_{\rm SO}^i+F_{\rm SO}^{i-1}}{(\Delta z)^2}=EF_{\rm SO}^i\ , \quad (22d)$$

where the superscripts denote the position along the growth axis within one period. The superscript l has been discarded. The Bloch condition is enforced by setting

$$F_j^{N+1}=F_j^{(1)}e^{iqd}\ , \quad (23a)$$

$$F_j^{(0)}=F_j^N e^{-iqd}\ , \quad (23b)$$

where $F_j^{(1)}$ denotes the function at the first point in the current unit cell, F_j^{N+1} is the function at the first point in the next unit cell, $F_j^{(0)}$ is function at the last point in the previous unit cell, d is the superlattice period, q is the crystal momentum along the growth axis, and j runs over the four bands. Close inspection of Eqs. (22a)–(22d) reveals that they form a system of equations resembling Eq. (16). Both the energies and wave functions can be obtained in a straightforward manner. Furthermore, the full coupling among the bands is retained, and the interface boundary conditions are automatically satisfied.

To demonstrate the reliability of our numerical technique, we have solved Eqs. (22a)–(22d) for the GaAs/$Ga_{1-x}Al_xAs$ system of Eppenga *et al.*[15] Using their set of parameters, we find that the calculated energies are identical to theirs for the test structure they analyzed. Additionally, with the use of an optimized set of parameters, we have since been able to obtain good agreement between the theoretically and experimentally determined transition energies for the GaAs/AlAs system.[26]

III. RESULTS

All of the physical constants required in the calculation are specified for the two binary compounds in Table I. Linear interpolation is utilized for intermediate mole fractions. The temperature dependence of these parameters has been neglected. The effective masses in Table I are close to those reported in Ref. 19 for bulk material. In all of the subsequent simulations, these parameters were not adjusted to fit the data of individual samples. Instead they were fixed for all of the samples we analyzed.

To test the validity of the model, we have calculated the Γ-point energies of a large number of superlattices and compared the energy differences with the published optical data for the corresponding structures. Table II relates the theoretical excitonic energies to the data of Ji *et al.*[6] The exciton binding energy has been subtracted from the calculated transition energies; a binding energy of 10 meV is assumed. The usual notation is employed: for instance, $1C$-$1H$ denotes the $n=1$ electron and $n=1$ hh exciton. It is clear that the theoretical values are in very good agreement with experiment. Offsets of 0.3 and 0.4 yield comparable energies for the e-hh excitons which are close to the experimental values. At the higher offset, the calculated energies for the $1C$-$1H$ exciton are consistently lower. For higher-order excitons the trend is more obscure and depends on the structure and composition of the superlattice.

Variations of the offset are liable to induce more substantial changes in the e-lh exciton energy. Greater sensitivity of the e-lh exciton energy to the offset can be expected due to the light holes residing in the GaAs layers for small offsets, and in the $In_xGa_{1-x}As$ layers for large offsets. This is illustrated more clearly in Figs. 1(a)–1(c) in which the energies of the e, hh, lh, and SO band edges are sketched along the growth axis for $Q_v=0.3$, 0.4, and 0.6. The band-edge profile is a strong function of both temperature and mole fraction. The temperature dependence is more striking in borderline cases. At 2 K the transition between direct and indirect e-lh excitonic behavior occurs at $Q_v\approx 0.45$. For offsets near 0.45 it is found that the e-lh exciton is direct at some temperatures and indirect at others. While the 0.3 offset yields reasonably close agreement with the data of Ref. 6, the theory is remarkably accurate for a 0.4 offset, the worst-case error being only 5 meV.

To verify the consistency of the model we computed the spectra of the samples of Ref. 1. The results are depicted in Table III. It is evident that the agreement is even closer. At 77 K the calculated energies are less sensitive to offset variations than at 2 K. Since both offsets produce very close fits, it is difficult to predict an offset value with great certainty. Once again, however, the agreement for the e-lh excitons is slightly closer for a 0.4 offset.

The previous two sets of data pertain to fairly thick structures. We have also tested the theory on thin samples. Table IV compares the measured data of Pan

TABLE I. The physical constants used in calculating the band structure. Except for the masses, all are taken from Ref. 19.

	d (Å)	dE_g/dP (10^{-6} eV/kg cm^2)	b (eV)	C_{11} (10^{11} dyn/cm^2)	C_{12} (10^{11} dyn/cm^2)	Δ (eV)	m_e/m_0	$m_{\rm hh}/m_0$	$m_{\rm lh}/m_0$	$m_{\rm SO}/m_0$
GaAs	5.6533	11.5	−1.7	11.88	5.380	0.341	0.067	0.454	0.08	0.15
InAs	6.0583	10.2	−1.8	8.329	4.526	0.381	0.023	0.410	0.04	0.08

TABLE II. Comparison with the experimental data of Ref. 6. All energies are expressed in eV. The data were measured at 2 K. (Sample designations are from Ref. 6.)

Sample	61	62	64	66	81
x	0.15	0.15	0.15	0.193	0.13
L_{GaAs}(Å)	200	200	200	200	200
$L_{In_xGa_{1-x}As}$	85	159	213	85	106
1*C*-1*H* (expt.)	1.3747	1.3604	1.3500	1.3334	1.3917
Theory (0.3 offset)	1.3798	1.3576	1.3514	1.3361	1.3913
Theory (0.4 offset)	1.3783	1.3571	1.3512	1.3346	1.3903
2*C*-2*H* (expt.)	1.4726	1.4059	1.3785	1.4393	1.4683
Theory (0.3 offset)	1.4768	1.4041	1.3810	1.4467	1.4652
Theory (0.4 offset)	1.4822	1.4022	1.3801	1.4398	1.4609
3*C*-3*H* (expt.)		1.4665	1.4293		
Theory (0.3 offset)		1.4697	1.4271		
Theory (0.4 offset)		1.4619	1.4247		
1*C*-1*L* (expt.)	1.4393	1.4179	1.4147	1.4115	1.4440
Theory (0.3 offset)	1.4275	1.4105	1.4054	1.3984	1.4343
Theory (0.4 offset)	1.4393	1.4232	1.4183	1.4144	1.4445

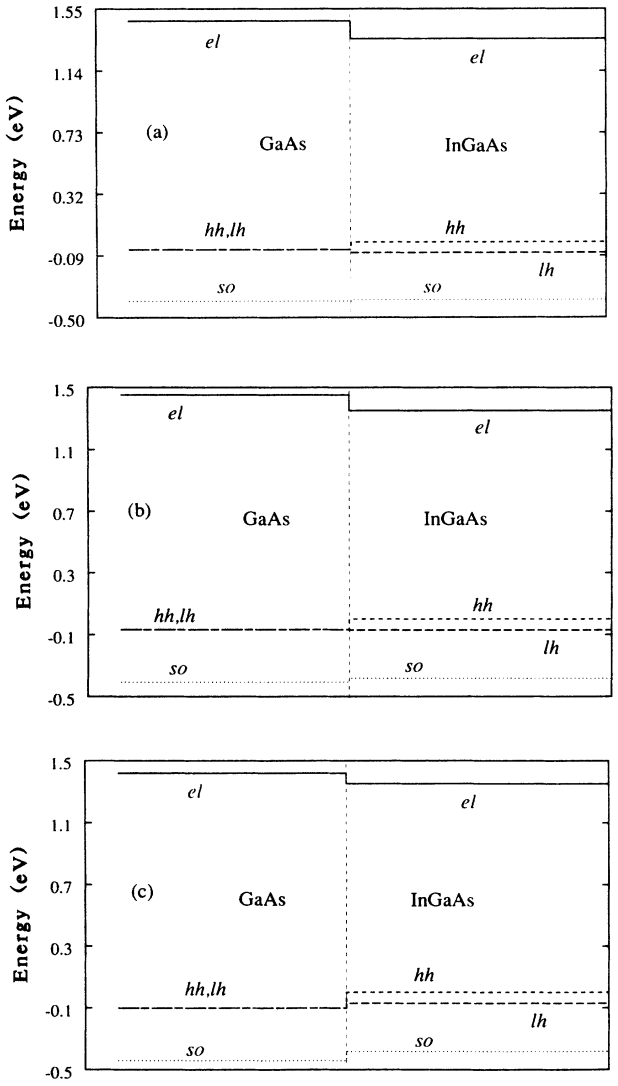

FIG. 1. The *e*, hh, lh, and SO band minima along the growth axis in the vicinity of the interface for Q_v=(a) 0.3, (b) 0.4, and (c) 0.6. The temperature is 2 K and the In mole fraction is 0.15.

et al.[8] with the calculated spectra. Unlike the previous two examples, the agreement is not as close. Yet the error is less than 0.8% in most cases. We have not attempted to vary the layer thicknesses to produce a better fit, choosing instead to use the nominal thicknesses: Pan *et al.*[8] have reported somewhat large thickness uncertainties in their structures. The agreement is close enough, we believe, to affirm the usefulness of the model for a wide range of structures. In this instance the calculated energies are relatively insensitive to offset variations at the higher temperatures. This, together with the lack of precise data regarding the geometry, makes it difficult to deduce an offset from the data of Ref. 8 alone.

The theory is especially effective in reproducing the spectra of Ref. 7, as shown in Table V. Based on an effective-mass theory with strain, Menendez *et al.*[7] had fitted their data to an offset of 0.6, i.e., with most of the band-gap difference appearing across the valence-band edge. This would imply complete type-I character, as illustrated in Fig. 1(c). Within our model, however, the calculated energy differences are relatively small for offset variations from 0.3 to 0.6. For example, the theoretical

TABLE III. Comparison with the 77-K experimental data of Ref. 1. The experimental numbers were estimated from the graphical data of Ref. 1.

	Sample		
	A	*B*	*C*
x	0.15	0.15	0.15
L_{GaAs} (Å)	200	200	200
$L_{In_xGa_{1-x}As}$	50	100	120
1*C*-1*H* (expt.)	1.397	1.369	1.360
Theory (0.3 offset)	1.411	1.375	1.369
Theory (0.4 offset)	1.408	1.374	1.368
2*C*-2*H* (expt.)		1.457	1.431
Theory (0.3 offset)	1.513	1.455	1.434
Theory (0.4 offset)	1.506	1.450	1.430
1*C*-1*L* (expt.)	1.451	1.428	1.415
Theory (0.3 offset)	1.447	1.421	1.416
Theory (0.4 offset)	1.454	1.433	1.428

TABLE IV. Comparison with the experimental data of Ref. 8. Sample 1 is (100 Å GaAs)/(50 Å $In_{0.11}Ga_{0.89}As$) and sample 2 is (100 ÅGaAs)/(30 Å $In_{0.12}Ga_{0.88}As$).

	Sample 1		Sample 2	
	300 K	77 K	300 K	77 K
1*C*-1*H* (expt.)	1.358	1.448	1.372	1.453
Theory (0.3 offset)	1.356	1.438	1.373	1.454
Theory (0.4 offset)	1.353	1.435	1.369	1.450
1*C*-2*H* (expt.)				1.487
Theory (0.3 offset)			1.401	1.481
Theory (0.4 offset)			1.406	1.485
1*C*-3*H* (expt.)	1.392	1.481		
Theory (0.3 offset)	1.387	1.468		
Theory (0.4 offset)	1.393	1.474		
2*C*-1*H* (expt.)			1.499	1.582
Theory (0.3 offset)			1.494	1.575
Theory (0.4 offset)			1.490	1.570
2*C*-2*H* (expt.)			1.528	1.616
Theory (0.3 offset)			1.523	1.602
Theory (0.4 offset)			1.525	1.605
2*C*-3*H* (expt.)	1.476	1.565		
Theory (0.3 offset)	1.493	1.573		
Theory (0.4 offset)	1.495	1.575		
1*C*-1*L* (expt.)	1.379	1.469	1.389	1.473
Theory (0.3 offset)	1.383	1.464	1.394	1.474
Theory (0.4 offset)	1.387	1.468	1.396	1.476
3*C*-3*H* (expt.)			1.560	1.646
Theory (0.3 offset)			1.557	1.636
Theory (0.4 offset)			1.556	1.635

energy for the 1*C*-1*H* exciton differs from the experimental value by 0.2 meV for $Q_v=0.6$. While the 0.3 offset prediction is furthest away for this exciton, it is an overestimate by only 1.1 meV, representing an error of 0.08%. For the 1*C*-1*L* exciton, the 0.6 offset prediction is most distant at 0.3% error while the 0.4 offset prediction is nearest at 0.06%.

Evidently any offset in the range 0.3–0.4 can accurately fit the available data. Our model appears to support an offset between 0.3 and 0.4, predicting a value nearer 0.4. Such an offset would mean that 1*C*-1*L* exciton is indirect in real space, a situation that is portrayed in Fig. 1(b).

It is instructive to examine the envelope functions as a function of Q_v for some of the superlattices described in the literature. Figures 2(a)–2(c) illustrate the envelope functions at $q=0$ and $Q_v=0.6$ for the structure of Ref. 7 for three different eigenvalues. Each state will, in general, consist of four components. But in the absence of hh-lh mixing the *e* and lh states contain three components and the hh states only a single component. Indirect coupling among all the bands still exists via the Luttinger parameters. In Fig. 2(a) the dominant component is the envelope function associated with the $|s\uparrow\rangle$ states. Based on the profile of the eigenvectors, the energy is assigned to the $n=1$ electron state. By a similar argument, Fig. 2(b) depicts the $n=1$ hh state and Fig. 2(c) the $n=1$ lh state. Type-I behavior is implied by the localization of the *e*, hh, and lh states in the $In_xGa_{1-x}As$ layer.

Figures 3(a)–3(c) show the ground-state envelope functions for $Q_v=0.4$. Contrary to expectations, the lh state is not localized in the GaAs layer but is extended over the entire period. Conditions are thus favorable for forming an *e*-lh exciton, and may serve to explain the strong 1*C*-1*L* peak reported in Ref. 7.

IV. SUMMARY

In summary, we have outlined a technique to calculate the band structure of strained $In_xGa_{1-x}As$-GaAs superlattices. The *e*, hh, lh, and SO bands are treated in a unified description in which Kane's **k·p** Hamiltonian

TABLE V. Comparison with the experimental data of Ref. 7. The structure is (415 Å GaAs)/(193 Å $In_{0.05}Ga_{0.95}As$). The measured data were taken at 5 K. The theoretical values were calculated for 2 K. The experimental numbers were estimated from the graphical data of Ref. 7. All energies are in eV.

Experiment		Theory		
Offset		0.3	0.4	0.6
1*C*-1*H*	1.4609	1.4620	1.4616	1.4607
2*C*-2*H*		1.4866	1.4851	1.4808
3*C*-3*H*		1.5067	1.5023	1.4926
1*C*-3*H*	1.4726	1.4728	1.4734	1.4736
1*C*-1*L*	1.4817	1.4784	1.4826	1.4859

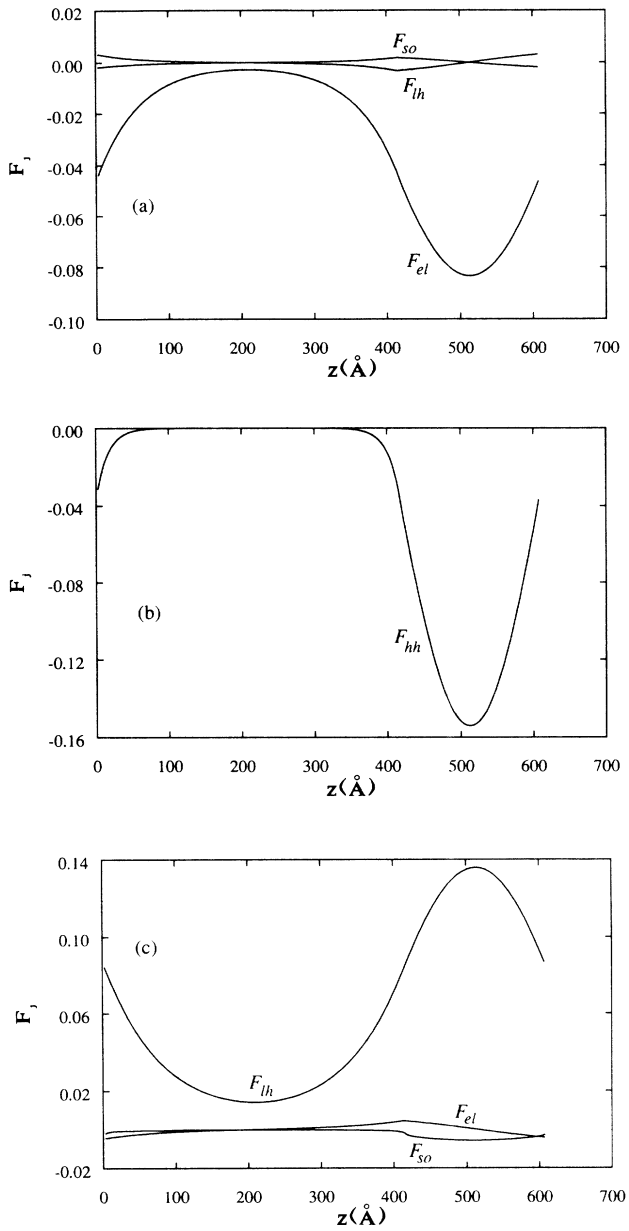

FIG. 2. Eigenvectors of the large matrix in Eq. (16) for E = (a) 1.4690 eV, (b) −0.001 655 3 eV, and (c) −0.026 877 eV. An offset of 0.6 is assumed. The superlattice is that of Ref. 7. The GaAs layer lies within $0 < z < 415$ Å and the $In_{0.05}Ga_{0.95}As$ layer is in the range $415 < z < 608$ Å. A temperature of 2 K is assumed. The eigenvalues represent the $n = 1$ e, hh, and lh states, respectively.

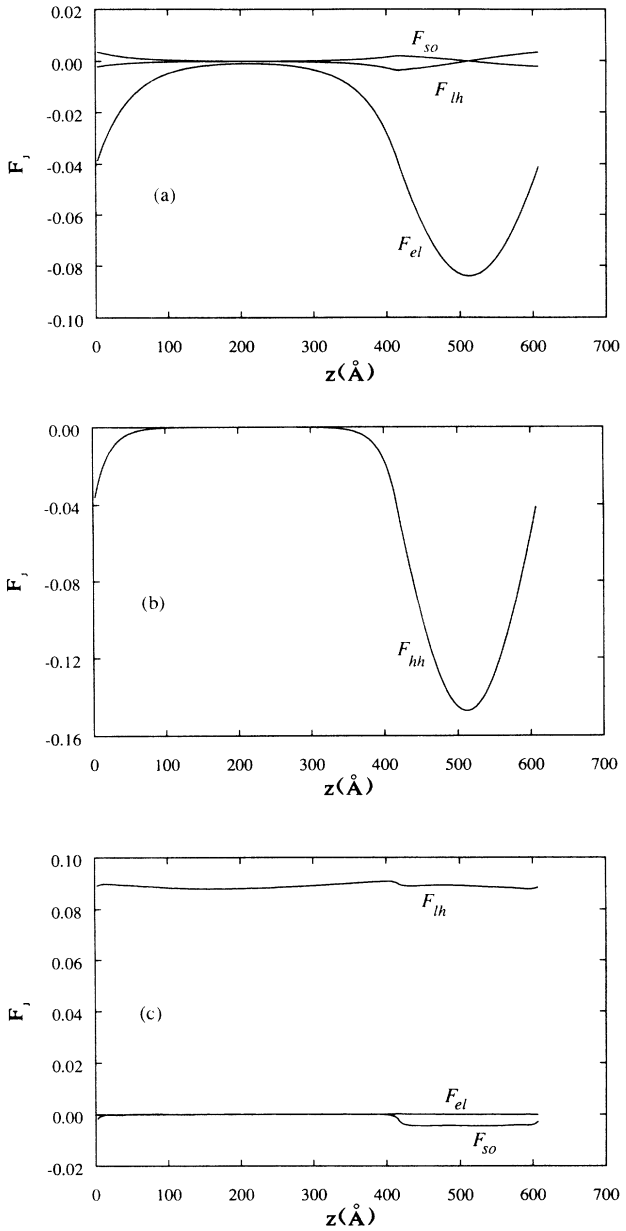

FIG. 3. Eigenvectors of the structure described in Fig. 2 for E = (a) 1.470 eV, (b) −0.001 551 8 eV, and (c) −0.022 574 eV. Here $Q_v = 0.4$. In each case the ground state is depicted.

containing the important free electron terms is combined with the strain Hamiltonian and diagonalized to produce the energies and wave functions. Four adjustable parameters are utilized to accurately simulate the bulk band structure of each host material. The calculated transition energies are in very good agreement with a wide range of published optical data at different temperatures for samples having mole fractions varying from 0.05 to 0.193. We find that the calculated transition energies are fairly insensitive to offset variations between 0.3 and 0.6. The e-hh excitonic energies can be fitted very well with any of these offsets. The calculated e-lh transition energies, however, appear to indicate an offset in the vicinity of 0.4.

ACKNOWLEDGMENTS

One of the authors (B.J.) is indebted to L. Liou for valuable discussions. The authors are grateful to K. Soda for helpful comments on the manuscript. This work was performed at the Electronic Technology Laboratory, Wright-Patterson Air Force Base, OH, under Contracts No. F33615-86-C-1050 (B.J.) and No. F33615-86-C-1062 (P.W.Y.), and was supported in part by the U.S. Air Force Office of Scientific Research.

[1]J. Y. Marzin, M. N. Charasse, and B. Sermage, Phys. Rev. B **31**, 8298 (1985).
[2]A. P. Roth, R. A. Masut, M. Sacilotti, P. J. D'Arcy, Y. Le Page, G. I. Sproule, and D. F. Mitchell, Superlatt. Microstruct. **2**, 507 (1986).
[3]N. G. Anderson, W. D. Laidig, R. M. Kolbas, and Y. C. Lo, J. Appl. Phys. **60**, 2361 (1986).
[4]U. K. Reddy, G. Ji, R. Houdre, H. Unlu, D. Huang, and H. Morkoç, Proc. Soc. Photo-Opt. Instrum. Eng. **794**, 116 (1987).
[5]G. Ji, D. Huang, U. K. Reddy, H. Unlu, T. S. Henderson, and H. Morkoç J. Vac. Sci. Technol. B **5**, 1346 (1987).
[6]G. Ji, U. K. Reddy, D. Huang, T. S. Henderson, and H. Morkoç, J. Appl. Phys. **62**, 3366 (1987).
[7]J. Menéndez, A. Pinczuk, D. J. Werder, S. K. Sputz, R. C. Miller, D. C. Sivco, and A. Y. Cho, Phys. Rev. B **36**, 8165 (1987).
[8]S. H. Pan, H. Shen, Z. Hang, F. H. Pollak, W. Zhuang, Q. Xu, A. P. Roth, R. A. Masut, C. Lacelle, and D. Morris, Phys. Rev. B **38**, 3375 (1988).
[9]M. J. Joyce, M. J. Johnson, M. Gal, and B. F. Usher, Phys. Rev. B **38**, 10 978 (1988).
[10]A. Ksendzov, H. Shen, F. H. Pollak, and D. P. Bour, in Proceedings of the 4th International Conference on Modulated Semiconductor Structures, Ann Arbor, 1989, edited by D. Tsui, L. L. Chang, and R. Merlin [Surf. Sci. (to be published)].
[11]J. Y. Marzin, *Heterojunctions and Semiconductors Superlattices,* edited by G. Allan, G. Bastard, N. Boccara, M. Lannoo, and M. Voos (Springer, Berlin, 1986), p. 161.
[12]G. Bastard, Phys. Rev. B **24**, 5693 (1981).
[13]M. F. H. Schuurmans and G.W. 't Hooft, Phys. Rev. B **31**, 8041 (1985).
[14]E. O. Kane, *Handbook on Semiconductors* (North-Holland, New York, 1982), Vol. I, p. 193.
[15]R. Eppenga, M. F. H. Schuurmans, and S. Colak, Phys. Rev. B **36**, 1554 (1987).
[16]J. M. Luttinger, Phys. Rev. **102**, 1030 (1956).
[17]F. H. Pollak and M. Cardona, Phys. Rev. **172**, 816 (1968).
[18]F. H. Pollak, Surf. Sci. **37**, 863 (1973).
[19]S. Adachi, J. Appl. Phys. **53**, 8875 (1982).
[20]Y. T. Leu, F. A. Thiel, H. Scheiber, B. I. Miller, and J. Bachman, J. Electron. Mater. **8**, 663 (1979).
[21]K. H. Goetz, D. Bimberg, H. Jür, J. Selders, A. V. Solomovon, G. F. Glinskii, M. Razeghi, and J. J. Robin, J. Appl. Phys. **54**, 4543 (1983).
[22]W. Porod, W. Pötz, and D. K. Ferry, J. Vac. Sci. Technol. B **3**, 1290 (1985).
[23]M. Altarelli, Physica B+C (Amsterdam) **117&118B**, 747 (1983).
[24]E. Merzbacher, *Quantum Mechanics,* 2nd ed. (Wiley, New York, 1970), pp. 80–113.
[25]R. A. Morrow and K. R. Brownstein, Phys. Rev. B **30**, 678 (1984).
[26]P. W. Yu, D. C. Reynolds, B. Jogai, and R. Jones (unpublished).